Review Article

*Lignin* **7**, 1-9 (2026)

DOI: https://doi.org/10.62840/lignin.7.0_1

The Lignin Society

*Lignin*

# Intrastem Behavior of Monolignol Glucosides Visualized by Cryo-Secondary Ion Mass Spectrometry

Dan Aoki[a,*] and Kazuhiko Fukushima[a]

[a]*Graduate School of Bioagricultural Sciences, Nagoya University, Nagoya 464-8601, Japan;*
**Corresponding author: aoki.dan@nagoya-u.jp*

*Received: 19 February 2026; revised in form: 4 March 2026; accepted: 10 March 2026*

**Abstract**

Monolignol glucosides occur in plants as water-soluble, chemically stabilized forms of monolignols and have been discussed as storage and transport forms in lignification. However, these small molecules readily change their localization during common analytical pretreatments, and therefore, discussions based on cell-level intact distributions within stems have been limited. In this review, we summarize prior efforts to reveal intrastem behavior using cryo-secondary ion mass spectrometry which directly visualizes the instantaneous distribution in freeze-fixed samples, together with (i) tissue assignment by microscopic observations, (ii) selection of target *m*/*z* values based on the ionization behavior of authentic standards, and (iii) validation by chromatography measurements of serial tangential sections. In addition, cryo-secondary ion mass spectrometry equipped with gas cluster ion beam measurements provides high-resolution and three-dimensional images. These approaches provide information on which tissues and cells contain what amounts of intrastem monolignol glucosides, and they contribute to re-examining and updating models for the transport, storage, and consumption of lignin precursors involved in lignin deposition.

***Keywords****: coniferin; imaging mass spectrometry; lignification; p-glucocoumaryl alcohol; syringin*

## INTRODUCTION

Lignin is an important polymer in the cell wall, and its formation differs widely across species, tissues, cell types, and positions within the cell wall. The formation mechanism is complex, and the interface between precursor biosynthesis and deposition into the cell wall is still a major unresolved issue [1–6]. While monolignols (MLs) are lignin precursors, in plants they are often glucosylated; protection of the phenolic OH group results in water-soluble and chemically stable forms (monolignol glucosides, MLG) [7–11]. To discuss the *in planta* roles of MLGs, high-resolution localization information is essential. However, the intact distribution of mobile small molecules is readily changed by typical procedures such as cutting, solvent exchange, resin embedding, and drying, making direct visualization of their microscopic distributions difficult. To close this gap, cryo-secondary ion mass spectrometry (cryo-SIMS), which directly measures the frozen-hydrated surface of freeze-fixed samples, has been established [12,13], enabling progress in discussions of MLG localization [14,15].

In this review, to treat cryo-SIMS data not as "a single image" but as "an interpretative framework," we compare findings from Ginkgo [16], Lilac [17], and Pinus [18,19] within an integrated framework by combining cryo-SIMS with three supporting approaches: (i) tissue assignment (microscopy), (ii) an *m*/*z* selection (ionization behavior of standard compounds and evaluation of interferential compounds), and (iii) liquid chromatography (LC)-based validation, thereby summarizing how far intrastem behavior of MLGs can currently be visualized.

## 2. EXPERIMENTAL FRAMEWORK

The analytical framework addressed in this review is summarized in Fig. 1. Below, we describe, based on these numbers, not the detailed procedures but rather what has become possible and what must be considered for interpretation.

*Lignin* **7**, 1-9 (2026)
DOI: https://doi.org/10.62840/lignin.7.0_1
The Lignin Society
*Lignin*

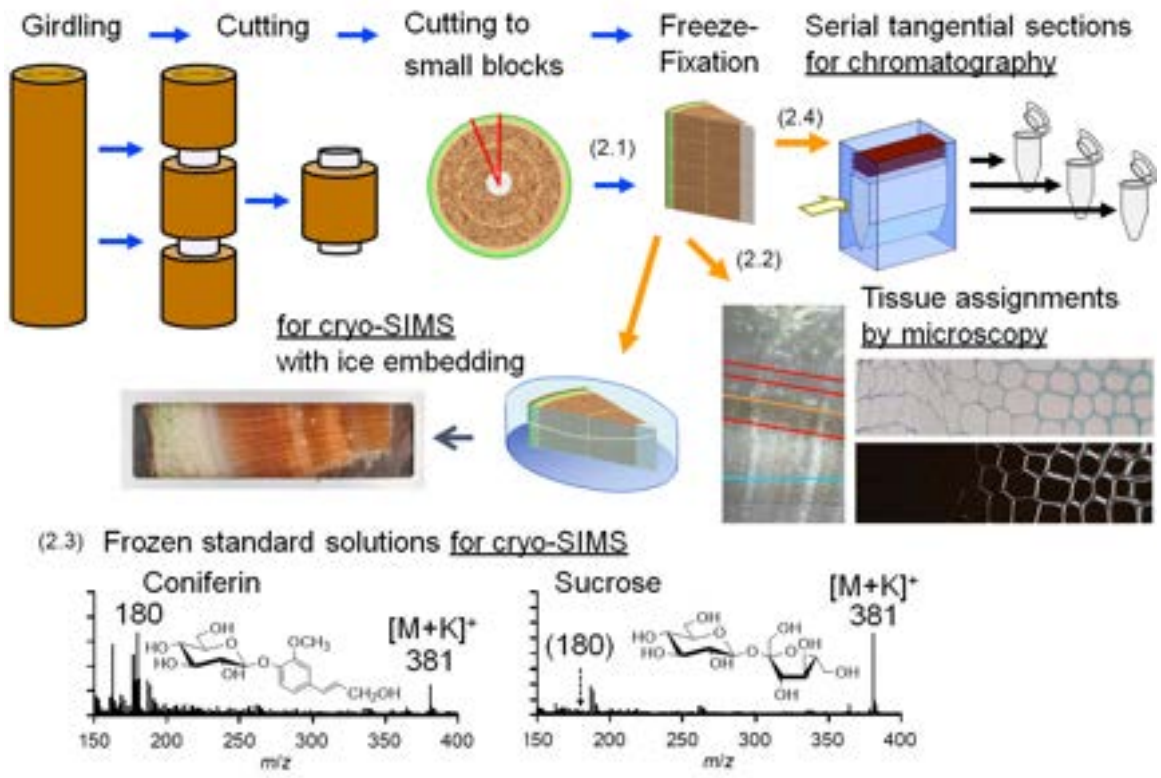


**Fig. 1.** Experimental framework of frozen-hydrated plant stem samples. The numbers (2.1)–(2.4) correspond to the section numbers in this paper.

### 2.1 Preservation of positional information by freeze fixation

The most important feature of cryo-SIMS is that it measures a sample in the frozen-hydrated state, allowing the intact localization of readily mobile compounds to be captured as a snapshot. However, especially for biological samples of a certain size, rapid subdivision of the sample block and rapid freezing methods are required to minimize ice-crystal formation and mobile component migration during sampling. In previous studies, sample blocks were rapidly frozen using liquid Freon R22 (−160°C) or dry ice/*n*-hexane, stored at −80°C, and then measured. Furthermore, after preparing a flat, clean surface for measurement using a cryomicrotome, it is necessary to promptly perform a low-temperature vacuum transfer or store the sample in liquid nitrogen to prevent sublimation from the surface.

### 2.2 Tissue and cellular assignment with microscopy

In analytical systems that couple cryo-SIMS with cryo-scanning electron microscopy (cryo-SEM), the same surface is observed by cryo-SEM (including freeze-etching) after the cryo-SIMS measurement, and positional information, such as the region from the cambial zone to differentiating xylem, is assigned. However, this does not necessarily provide sufficient information to understand tissue/cellular states or to compare discussion with previous reports. Therefore, for example, in the most recent report [19], sections were prepared using Kawamoto's adhesive film method [20,21], and chemical distribution was discussed with support from the organization of cell-wall formation stages based on microscopic observations.

### 2.3 Compound assignment

Table 1 summarizes examples of secondary ions for MLs, MLGs, and related compounds detectable in plants. Specialized metabolites in plants have quite various structures but often the nominal

*Lignin* **7**, 1-9 (2026)
DOI: https://doi.org/10.62840/lignin.7.0_1
The Lignin Society
*Lignin*

values of their secondary ions are unfortunately the same. Because cryo-SIMS generally provides only mass spectra acquired by a time-of-flight single-detector system, it is difficult to identify compounds; at a minimum, the following steps are required.

- Confirmation of ionization behavior of target compounds by cryo-SIMS measurement of frozen-hydrated standards.
- Interference evaluation based on standard spectra and assumed co-detectable compounds, and selection of *m*/*z* values to be used for visualization.
- Qualitative and quantitative validation by LC and related methods (See section 2.4).

For example, for coniferin (CF), the molecular ion *m*/*z* 381 as a $K^+$ adduct overlaps with the $K^+$ adduct of sucrose and therefore cannot be used. However, based on the mass spectrum of CF in which the α-position of coniferyl alcohol is $^{13}$C-labeled, it was found that the *m*/*z* 180 ion originates not from glucose but from the coniferyl alcohol moiety (an aglycone-derived fragment ion), and it was shown to be usable as a visualization indicator of CF.

**Table 1.** Secondary ion examples for cryo-SIMS visualization

| Category | Compound | Positive ion | Negative ion |
|---|---|---|---|
| metallic | metallic element [22,23] | $[M]^+$ | - |
| neutral | mono/di-saccharide [16–18,24,25] | $[M+K]^+$ | $[M-H]^-$, $[M+Cl]^-$ |
| acidic | monolignol [16–18, 24] | $[M-OH]^+$, $[M]^+$, $[M+K]^+$ | $[M-H]^-$ |
| neutral | monolignol glucoside [16–19,24,25] | [aglycone]$^+$, $[M+K]^+$ | [aglycone−H]$^-$, $[M-H]^-$, $[M+Cl]^-$ |
| acidic | lignan [25] | $[M+K]^+$ | $[M+H]^-$ |
| neutral | lignan glucoside [25] | $[M+K]^+$, [fragment]$^+$ | - |
| acidic | fatty acid [26] | - | $[M-H]^-$ |
| acidic | flavonoid (catechin) [27] | $[M]^+$ | - |
| acidic | stilbenoid, stilbene glucoside [28] | $[M]^+$, $[M+H]^+$, [fragment]$^+$ | $[M]^-$, $[M-H]^-$, [fragment]$^-$ |
| acidic | terpenoid (feruginol, [12] taxane [29]) | $[M]^+$ | - |
| basic | amine [30] | $[M+H]^+$, [fragment]$^+$ | - |
| ionic | phosphatidylcholine [14–19,29,31,32] | [fragment]$^+$ | - |
| ionic | quaternary ammonium [24,32] | $[M]^+$ | - |
| neutral | water [33] | $[(H_2O)_n+H]^+$ | $[(H_2O)_n-H]^-$ |

In the case of the angiosperm Lilac, because the *m*/*z* 180 ion can also arise from syringin, it is difficult to visualize CF and syringin in the same sample independently, and discussion has therefore been limited to the distribution of syringin alone (*m*/*z* 210 and 411 ions). Regarding these *m*/*z* interference situations, TOF-SIMS instruments equipped with tandem mass spectrometry or ultrahigh mass-resolution modules have recently been commercialized. They are expected to be useful for simultaneous visualization of various compounds [34–36].

SIMS ion intensities are strongly affected by the surrounding environment (e.g., a matrix such as inorganic elements). In plant tissues rich in K [37], K-adduct ions are readily generated; however, it is also necessary to ensure agreement with the K distribution. In addition, because ionization yields differ considerably among compounds, quantitative discussion is difficult only by SIMS data, and combination with other analyses, as described in the next section, is required.

### 2.4 Qualitative/quantitative analysis and coarse distribution evaluation

By cutting serial tangential sections from freeze-fixed samples and analyzing extracts by LC (and, where applicable, ion exchange chromatography (IEC), LC-MS, etc.), the amount and coarse

*Lignin* **7**, 1-9 (2026)
DOI: https://doi.org/10.62840/lignin.7.0_1
The Lignin Society
*Lignin*

radial distribution of target compounds can be confirmed. In this context, the position of the cambial zone has been determined based on the dry weight of each section. In the latest report [19], via incorporating a cryo-microdissection (cryo-MD) process in which the cross section is observed and recorded during cutting and each tangential section is assigned to a cell-wall formation stage, the positional assignment of each section became more accurate.

## 3. CASE STUDIES

### 3.1 *Ginkgo biloba* [16,25]

In freeze-fixed stems of Ginkgo, the CF-derived *m*/*z* 180 ion was shown to localize in differentiating xylem adjacent to the cambial zone (Fig. 2a). Moreover, the radial distribution of CF obtained by LC was consistent with the radial profile of *m*/*z* 180, providing a basis for image interpretation. In Ginkgo, CF accumulates in tracheid cells of differentiating xylem, consistent with its assimilation into lignin shown in previous $^{14}$C-labeled CF feeding experiments, suggesting that CF is likely utilized as a lignin precursor [38].

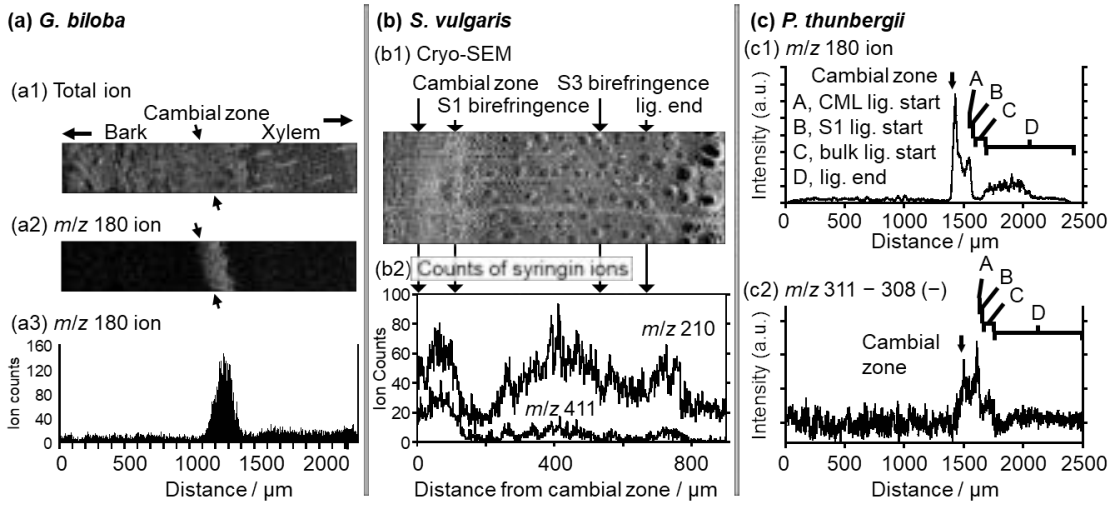


**Fig. 2.** MLG distributions for (a) *G. biloba*, (b) *S. vulgaris*, and (c) *P. thunbergii* stems. (a): (a1) Total ion, (a2) *m*/*z* 180 ion, and (a3) a line profile of the *m*/*z* 180 ion. (b): (b1) A cryo-SEM image and (b2) counts for syringin ions at *m*/*z* 210 and *m*/*z* 411. (c): Line profiles of (c1) the *m*/*z* 180 ion and (c2) the difference between the *m*/*z* 311 ion and the *m*/*z* 308 ion. The lignification (lig.) stages of the cell wall of the tracheid are presented by A, B, C, and D.

### 3.2 *Syringa vulgaris* [17]

In *S. vulgaris* (Lilac), quantitative LC analysis using serial tangential sections of freeze-fixed samples showed that both CF and syringin were mainly abundant in bark and were detected in small amounts from the cambial zone to differentiating xylem. Cryo-SIMS/SEM revealed that syringin was found mainly in the phloem (Fig. 2b). In contrast, within the xylem, it was broadly distributed across cell types from the cambial zone through early differentiation stages. Furthermore, in vessels characteristic of hardwoods, syringin was detected from vessel sap even though those vessels should already have completed lignification. It is unclear whether this syringin is used for lignification of surrounding cells or indicates transport to more distant sites.

When isotope-labeled syringin is fed to Lilac, incorporation into lignin in differentiating xylem has already been reported [39]. Therefore, these results show that syringin is likely stored in large amounts in the phloem as a defensive phenolic glucoside or as a precursor to other compounds. In contrast, in the xylem, it is used in concert with cell wall formation and lignification. Based on standard spectra,

*Lignin* **7**, 1-9 (2026)
DOI: https://doi.org/10.62840/lignin.7.0_1
The Lignin Society
*Lignin*

syringin can be visualized by *m*/*z* 411 ($[M+K]^+$) and *m*/*z* 210 (aglycone). CF *m*/*z* 381 ($[M+K]^+$) overlaps with that of disaccharides (especially sucrose), and because *m*/*z* 180 can also be generated from syringin, independent visualization of the two was difficult.

### 3.3 *Pinus thunbergii* [18)]

In a study comparing compression wood and opposite wood of Pinus, the position of the cambial zone and lignification stages of tracheids were determined by observations by cryo-SEM and visible, polarized, and UV microscopy, and cryo-SIMS images were discussed in an integrated manner with distributions obtained by LC/IEC. CF (*m*/*z* 180) localized in differentiating xylem adjacent to the cambial zone, was high at lignification stages corresponding to the compound middle lamella (CML) and S1 layer, and then decreased sharply near the onset of bulk lignification. This stage-dependent increase and decrease is comparable to CF localization in Ginkgo.

After examining interferences from other compounds, finally, CF was visualized using *m*/*z* 180 (+), while *p*-glucocoumaryl alcohol (PG) was visualized using the difference between *m*/*z* 311, corresponding to $[M-H]^-$, and the background signal at *m*/*z* 308 (Fig. 2c). The distribution of PG within the Pinus stem was similar to that of CF and was detected in the region from the cambial zone to differentiating xylem. The degree of sharp decrease near the onset of bulk lignification was milder than that of CF. As also indicated in feeding experiments with isotope-labeled precursors, the behaviors of CF and PG in differentiating xylem may be individually regulated [40,41)]. This is consistent with a recent report using fluorescently labeled MLs, which proposes that the oxidative deposition activities of G and H units may also be enzymatically controlled [18,42)].

Across the three species described above, previous studies have reported that isotope-labeled MLGs fed to plants are assimilated in differentiating xylem in the same manner as normal lignin deposition [11,38–41)]. In the present work, we showed that MLGs are indeed present near the relevant sites and that the apparent stored amounts decrease in accordance with lignification stages [16–19)]. Based on these results, we believe that MLGs function as a storage form for lignin precursors. On the other hand, whether glucosides must necessarily be involved as an obligatory route is not yet proven [2,11,43)]. In addition, further improvements in sensitivity and spatial resolution are required to elucidate details of intercellular and intracellular transport of MLs and MLGs.

### 3.4 Toward higher spatial resolution and three-dimensional visualization

In the latest report [19)], two approaches were used to discuss MLs and MLGs in Pinus at higher resolution further: (i) assigning serial tangential sections to cell-wall formation stages by cryo-MD and analyzing their extracts by LC-MS, and (ii) visualizing CF distributions at higher spatial resolution by cryo-SIMS equipped with a gas cluster ion beam (GCIB).

In approach (i), from LC-MS results, a classification of chemical forms was again presented, in which CF and PG are the major storage forms, coniferyl alcohol is minor, and *p*-coumaryl alcohol is detected in mature xylem. However, it was shown that within a three-dimensional sample block, stages of cell-wall formation are not necessarily perfectly parallel, making it difficult to obtain tangential sections composed solely of cells at a single stage.

In approach (ii), cryo-GCIB-SIMS visualized high-resolution localization of CF. CF (*m*/*z* 180) existed at high local concentrations as “storage domains” near the cell wall around the boundary from the cell expansion zone to the secondary wall (SW) thickening zone (Fig. 3). Moreover, 3D images obtained by repeating surface analysis and GCIB sputtering showed that these CF storage domains are continuously distributed along the cell axis over approximately 10–20 μm. However, at present, the most convincing accumulation of high-resolution and 3D evidence is for CF, and limitations in the *m*/*z* selection and sensitivity remain for PG.

*Lignin* **7**, 1-9 (2026)
DOI: https://doi.org/10.62840/lignin.7.0_1
The Lignin Society
*Lignin*

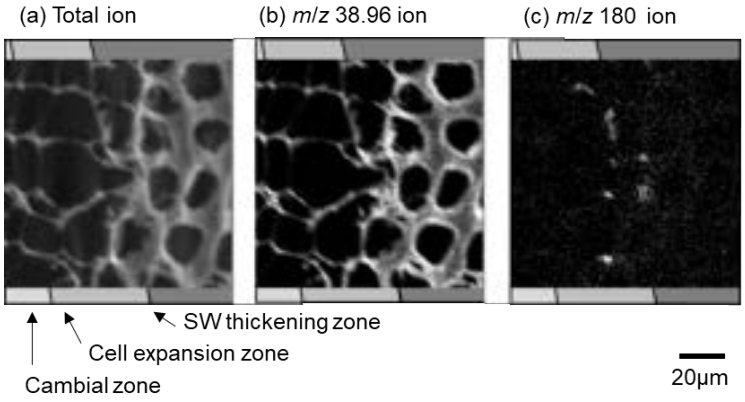


**Fig. 3.** Cryo-GCIB-SIMS images of (a) total ion, (b) the *m*/*z* 38.96 ion, and (c) the *m*/*z* 180 ion. Grayscale indicates the positions of the cambial zone, cell expansion zone, and secondary wall (SW) thickening zone.

## 4. REMARKS

### 4.1 "Where" they are: tissues and cell populations

Comparisons among the three species indicate that MLGs are not uniformly distributed within stems but present in "living cell populations" from the cambial zone to the differentiating xylem. CF in Ginkgo/Pinus is prominent in differentiating xylem adjacent to the cambial zone. At the same time, in Lilac, it is dominant in the phloem but is also detected in xylem in a differentiation-stage-dependent manner.

### 4.2 "When" they appear: correspondence with cell-wall formation and lignification stages

In Pinus, CF is abundant at lignification stages corresponding to the CML/S1 and decreases sharply near the onset of bulk lignification, clarifying its response along the time (formation stage) axis. Cryo-MD and LC-MS can be positioned as techniques that connect detailed microscopic observations and quantitative chemical data, with the differentiation stage as the primary axis [19].

### 4.3 "How to interpret" them: updated points in the storage and supply model

At present, what can be stated is the fact that MLGs accumulate in specific regions from the cambial zone to differentiating xylem and increase or decrease in a stage-dependent manner. To connect this to a precursor supply model, spatial consistency is required among deglucosylation (e.g., β-glucosidases), transport (intercellular and intracellular), and radical coupling reactions on the cell-wall side. The observation of the CF storage domain in Pinus (near the cell wall at the Ez/SWt boundary) may provide an opportunity to reconsider supply pathways beyond a simple "vacuolar storage" picture. In particular, further studies are needed to determine whether lignin can be deposited across the entire cell wall in the same manner as from highly localized storage domains, and what mechanisms would be required for that.

### 4.4 Future directions

- High mass resolution and MS/MS to resolve *m*/*z* interferences: separation of CF/sucrose and improvement of specificity for candidate PG ions.
- Strengthening linkage to "quantification": standardization of stage assignment, LC quantification, interpretation of images, as in cryo-MD and LC-MS, within the same individual and the same position.

- Fine distributions of PG and syringin: based on the current CF-centered status, redesign of *m*/*z* selection and validation design to obtain high-resolution images for PG/syringin, and further examination toward higher sensitivity for imaging trace components.
- Biological integration: the need to connect spatial information on enzymes (glucosyl transferases/β-glucosidases, etc.), transport, and cell-wall reactions with MLG distributions in the same individual [1,2,10,19,43–49].

## 5. CONCLUSIONS

1. Using an analytical framework centered on cryo-SIMS that combines "tissue assignment, *m*/*z* selection, LC-based validation," it became possible to compare intrastem behavior of MLGs and to concretize, mainly for CF, a picture of storage in differentiating xylem adjacent to the cambial zone.
2. In the future, resolving *m*/*z* interferences and strengthening linkage to quantification, as well as addressing the fine distributions of PG and syringin, as well as those of each ML, will directly contribute to re-examining models of lignification in differentiating xylem cell walls.

## ACKNOWLEDGEMENTS

This study was supported by JSPS KAKENHI Grant Numbers JP21228004, JP22580188, JP25252032, JP25114508, JP15H01230, JP15K07510, JP18H03959, JP20H03044, JP23K26968, and JP24H00056.

## REFERENCES

1) Boerjan, W. *et al*., Lignin biosynthesis. *Annu. Rev. Plant Biol.* **54**, 519–546 (2003).
2) Vanholme, R. *et al*., Lignin biosynthesis and structure. *Plant Physiol*. **153**, 895–905 (2010).
3) Weng, J. K., Chapple, C., The origin and evolution of lignin biosynthesis. *New Phytol*. **187**, 273–285 (2010).
4) Barros, J., *et al*., The cell biology of lignification in higher plants. *Ann. Bot.* **115**, 1053–1074 (2015).
5) Meents, M. J. *et al*., The cell biology of secondary cell wall biosynthesis. *Ann. Bot.* **121**, 1107–1125 (2018).
6) Tobimatsu, Y., Schuetz, M., Lignin polymerization: How do plants manage the chemistry so well? *Curr. Opin. Biotechnol.* **56**, 75–81 (2019).
7) Freudenberg, K. & Harkin, J. M., The glucosides of cambial sap of spruce. *Phytochemistry* **2**, 189–193 (1963).
8) Terazawa, M. *et al*., Phenolic compounds in living tissue of woods. I. Phenolic β-glucosides of 4-hydroxycinnamyl alcohol derivatives in the cambial sap of woods. *Mokuzai Gakkaishi*. **30**, 322–328 (1984).
9) Savidge, R. A., Coniferin, a biochemical indicator of commitment to tracheid differentiation in conifers. *Can. J. Bot.* **67**, 2663–2668 (1989).
10) Dharmawardhana, D. P. *et al*., A β-glucosidase from lodgepole pine xylem specific for the lignin precursor coniferin. *Plant Physiol.* **107**, 331–339 (1995).
11) Terashima, N. *et al*., Monolignol glucosides as intermediate compounds in lignin biosynthesis. Revisiting the cell wall lignification and new 13 C-tracer experiments with *Ginkgo biloba* and *Magnolia liliiflora*. *Holzforschung* **70**, 801–810 (2016).
12) Kuroda, K. *et al*., The cryo-TOF-SIMS/SEM system for the analysis of the chemical distribution in freeze-fixed *Cryptomeria japonica* wood. *Surf. Interface Anal*. **45**, 215–219 (2013).
13) Masumi, T. *et al*., Adsorption behavior of poly(dimethyl-diallylammonium chloride) on pulp fiber studied by cryo-time-of-flight secondary ion mass spectrometry and cryo-scanning electron microscopy. *Appl. Surf. Sci*. **289**, 155–159 (2014).

14) Aoki, D. *et al*., Cryo secondary ion mass spectrometry for wood component visualization: a mini review. *Holzforschung* **76**, 145–154 (2022).
15) Aoki, D., Fukushima, K., Visualization of mobile components by secondary ion mass spectrometry. *Mokuzai Gakkaishi.* **72**, *in press* (2026).
16) Aoki, D. *et al*., Distribution of coniferin in freeze-fixed stem of *Ginkgo biloba* L. by cryo-TOF-SIMS/SEM. *Sci. Rep*. **6**, 31525 (2016).
17) Aoki, D. *et al*., Microscopic distribution of syringin in freeze-fixed *Syringa vulgaris* stems. *Plant Direct* **3**, 1–8 (2019).
18) Maeda, N. *et al*., The distribution of monolignol glucosides coincides with lignification during the formation of compression wood in *Pinus thunbergii*. *Plant J*. **121**, e17209 (2025).
19) Aoki, D. *et al*., Storage domains of coniferin in cell wall forming tracheid cells in *Pinus thunbergii* stems evaluated by cryo microscopic chemical analyses. *Sci. Rep.* **15**, 38977 (2025).
20) Kawamoto, T., Use of a new adhesive film for the preparation of multi-purpose fresh-frozen sections from hard tissues, whole-animals, insects and plants. *Arch. Histol. Cytol.* **66**(2), 123–143 (2003).
21) Kawamoto, K. *et al*., A study of bone formation around titanium implants using frozen sections. *J. Hard Tissue Biol.* **30**(2), 165–174 (2021).
22) Zheng, P. *et al*., Determination of inorganic element distribution in the freeze-fixed stem of $Al_2(SO_4)_3$-treated *Hydrangea macrophylla* by TOF-SIMS and ICP-AES. *Holzforschung* **71**(6), 471–480 (2017).
23) Aoki, D. *et al*., Translocation of $^{133}Cs$ administered to *Cryptomeria japonica* wood. *Sci. Total Environ.* **584**–**585**, 88–95 (2017).
24) Okumura, W. *et al*., Distribution of salicifoline in freeze-fixed stems of *Magnolia kobus* as observed by cryo-TOF-SIMS. *Sci. Rep*. **7**, 5939 (2017).
25) Yu, M. *et al*., Distribution of lignans and lignan mono/diglucosides within *Ginkgo biloba* L. stem. *Phytochemistry* **196**, 113102 (2022).
26) Yamagishi, S. *et al*., Artifactual lipid coatings on intervessel pit membranes in dried xylem tissues of some angiosperms. *IAWA J*. **42**(4), 365–383 (2021).
27) Jyske, T. *et al*., Localization of (+)-Catechin in *Picea abies* phloem: responses to wounding and fungal inoculation. *Molecules* **25**, 2952 (2020).
28) Jyske, T. *et al*., In planta localization of stilbenes within *Picea abies* phloem. *Plant Physiol*. **172**, 913–928 (2016).
29) Gong, Q. *et al*., Microscopic distribution of taxanes in freeze-fixed stems of *Taxus cuspidata*. *Front. Chem*. **12**, 1437141 (2024).
30) Oota, M. *et al*., Identification of naturally occurring polyamines as root-knot nematode attractants. *Mol. Plant* **13**, 658–665 (2020).
31) Roddy, T. P. *et al*., Identification of cellular sections with imaging mass spectrometry following freeze fracture. *Anal. Chem.* **74**(16), 4020–4026 (2002).
32) Gong, Q. *et al*., Microscopic distribution of alkaloids in freeze-fixed stems of *Phellodendron amurense*. *Front. Plant Sci.* **14**, 1203768 (2023).
33) Ito, T. *et al*., Direct mapping of hydrangea blue-complex in sepal tissues of *Hydrangea macrophylla*. *Sci. Rep.* **9**, 5450 (2019).
34) Smith, D. F. *et al*., High mass accuracy and high mass resolving power FT-ICR secondary ion mass spectrometry for biological tissue imaging. *Anal. Bioanal. Chem*. **405**, 6069–6076 (2013).
35) Fisher, G. L. *et al*., A new method and mass spectrometer design for TOF-SIMS parallel imaging MS/MS. *Anal. Chem*. **88**, 6433–6440 (2016).
36) Passarelli, M. K. *et al*., The 3D OrbiSIMS—label-free metabolic imaging with subcellular lateral resolution and high mass-resolving power. *Nat. Methods* **14**(12), 1175–1183 (2017).
37) Kirkby, E., Introduction, definition and classification of nutrients. "Marschner's mineral nutrition of higher plants" 3rd ed., Marschner, H. ed., Academic Press, Amsterdam, 2012, pp. 3–5.
38) Fukushima, K., Terashima, N., Heterogeneity in formation of lignin XIV. Formation and structure of lignin in differentiating xylem of *Ginkgo biloba*. *Holzforschung* **45**, 87–94 (1991).

*Lignin* **7**, 1-9 (2026)
DOI: https://doi.org/10.62840/lignin.7.0_1
The Lignin Society
*Lignin*

39) Fukushima, K., Terashima, N., Heterogeneity in formation of lignin. XIII. Formation of *p*-hydroxyphenyl lignin in various hardwoods visualized by microautoradiography. *J. Wood Chem. Technol.* **10**, 413–433 (1990).
40) Terashima, N., Fukushima, K., Heterogeneity in formation of lignin – XI: an autoradiographic study of the heterogeneous formation and structure of pine lignin. *Wood Sci. Technol.* **22**, 259–270 (1988).
41) Fukushima, K., Terashima, N., Heterogeneity in formation of lignin. Part XV: formation and structure of lignin in compression wood of *Pinus thunbergii* studied by microautoradiography. *Wood Sci. Technol.* **25**, 371–381 (1991).
42) Hiraide, H. *et al*., Localised laccase activity modulates distribution of lignin polymers in gymnosperm compression wood. *New Phytol*. **230**, 2186–2199 (2021).
43) Le Roy, J. *et al*., Glycosylation is a major regulator of phenylpropanoid availability and biological activity in plants. *Front. Plant Sci*. **7**, 735 (2016).
44) Tsuyama, T. *et al*., Proton-dependent coniferin transport, a common major transport event in differentiating xylem tissue of woody plants. *Plant Physiol.* 162, 918–926 (2013).
45) Chou, E.Y. *et al*., Distribution, mobility, and anchoring of lignin-related oxidative enzymes in Arabidopsis secondary cell walls. *J. Exp. Bot*. **69**, 1849–1859 (2018).
46) Perkins, M. *et al*., The transport of monomers during lignification in plants: anything goes but how? *Curr. Opin. Biotechnol.* **56**, 69–74 (2019).
47) Tsuyama, T. *et al*., Proton gradient-dependent transport of *p*-glucocoumaryl alcohol in differentiating xylem of woody plants. *Sci. Rep.* **9**, 8900 (2019).
48) Hoffmann, N. *et al*., Laccases and peroxidases co-localize in lignified secondary cell walls throughout stem development. *Plant Physiol*. **184**, 806–822 (2020).
49) Tsuyama, T., Lignin monomer transport in seed plants. *Lignin*. **6**, 1–10 (2025).